J. Phys.: Condens. Matter 5 (1993) 267–282. Printed in the UK

A new fast spherical approximation for calculation of multiple-scattering contributions in x-ray absorption fine structure and its application to ReO_3, $NaWO_3$ and MoO_3

A Kuzmin and J Purans
Institute of Solid State Physics, University of Latvia, LV-1063 Riga, Latvia

Received 1 April 1992, in final form 20 October 1992

Abstract. We present a new fast spherical approximation (FSA) for the calculation of multiple-scattering contributions in x-ray absorption fine structure. The experimental XAFS spectra of the Re L_3 edge in ReO_3, the W L_3 edge in $NaWO_3$ and the Mo K edge in MoO_3 are analysed by the new approach. It is shown that the FSA gives good results for their description both in the high and low energy ranges.

1. Introduction

The method of x-ray absorption spectroscopy, rapidly developed in the last years, allows one to obtain unique and detailed information about the electronic structure and the local environment around the absorbing centre, despite the existence or absence of ordering in the system [1]. This information is contained in the oscillatory structure of the absorption coefficient, called x-ray absorption fine structure (XAFS). The physical reason for the appearance of oscillations is scattering of the outgoing photoelectron wave by atoms surrounding the absorbing centre. The modern theory of XAFS, based on the formalism of multiple-scatterings (MS) [2], allows the possibility of obtaining the information about two-, three- and four-body correlation functions [3]. In the frequently used single-scattering (SS) approximation, this latter information is lost, and in addition, sometimes this approach fails or leads to large errors in the amplitude and in the phase of the XAFS function [4]. The important role of MS processes was discovered for the first time in the so-called 'focusing' or 'shadowing' effect; that is, the great increase of the photoelectron wave amplitude in linear or nearly collinear atomic chains [5, 6]. In addition to this they become very important at low photoelectron energies near the absorption edge. This region, called the x-ray absorption near edge structure, must be analysed in the general case in the framework of the full multiple-scattering (FMS) approach [7].

The exact curved-wave approach [5, 8] to the MS calculations and its simplified and more rapid version for the angle-averaged case (the fast curved-wave method (FCW)) [7, 8] are in reality very time-consuming computationally and thus cannot be widely used in routine structural analysis of unknown compounds. This fact has led to the appearance of different approximations [8–13], which are simpler and faster than the FCW. However, up to now there has not been sufficient work done, in which they have been applied and tested for different compounds. It is known that

0953-8984/93/030267+16$07.50

the most simple approach, based on the plane-wave approximation (PWA) [12], leads to significant errors both in the phase and in the amplitude of the XAFS function especially at low energies, where MS signals make the main contribution. Because of this it cannot be used for MS calculations without loss of accuracy. The better approximations, such as the modified small-scattering-centre approximation (MSSCA) and the more precise reduced angular-momentum expansion (RAME) [9, 10], did not give good enough agreement with experimental data either [14, 15].

In this paper we present a new fast spherical approximation (FSA) for the calculation of multiple-scattering contributions in x-ray absorption fine structure and demonstrate its use for three crystalline systems (ReO_3, $NaWO_3$ and MoO_3) with different local symmetry and high contribution of MS processes. The new approach works as fast as the PWA, but gives good results both in the high- and low-energy ranges.

The experimental details and data treatment procedure are described in section 2. In section 3 the procedure of the cluster potential construction and scattering matrix elements calculation is presented. Section 4 describes the new FSA for the MS contribution calculation. The applications of the new approach to three compounds (ReO_3, $NaWO_3$ and MoO_3) are considered in section 5. A summary and main conclusions are in section 6.

2. Experiment and data analysis

The x-ray absorption spectra of the Re L_3 edge in ReO_3, the W L_3 edge in $NaWO_3$ and the Mo K edge in MoO_3 were measured in transmission mode at room temperature at the ADONE storage ring (the Italian National Synchrotron Centre at Frascati) on the BX-1 PWA beamline with utilization of the synchrotron radiation from the wiggler source. The storage ring ADONE operated at 20–50 mA and 1.5 GeV with a wiggler current of 4000 A. Two channel-cut crystal monochromators (Si[111] and Si[220]) were used. The results of the analysis of the first coordination shell in the single-scattering PWA with amplitudes and phases calculated in the spherical wave approximation (SWA) by McKale *et al* [16] were published by us earlier [17]. Note that the obtained structural parameters are in a good agreement with the x-ray diffraction data.

The experimental spectrum treatment was carried out following a now standard procedure [18]. The background contribution from previous edges $\mu_B(E)$ was approximated according to the Victoreen rule [19] ($\mu_B = A/E^3 + B/E^4$) and subtracted from the experimental spectrum $\mu(E)$. After that, the atomic-like term $\mu_0(E)$ was found by a cubic-spline approximation, and the XAFS signal $\chi(k)$ was determined as $\chi(k) = (\mu - \mu_B - \mu_0)/\mu_0$, where the photoelectron wavevector k is defined as $k = \sqrt{(2m/\hbar^2)(E - E_0)}$ (m is the electron mass and $\hbar$ is Planck's constant). The energy origin E_0, corresponding to the continuum threshold, was chosen past the first strong resonance ('white line') at 15 eV above the inflection point of the absorption edge for the Re and W L_3 edges and at the inflection point of the absorption edge past the pre edge shoulder in the case of the Mo K edge. Thus, in both cases, the E_0 positions were chosen according to the features corresponding to quasibound excited states. The Fourier transform (FT) procedure with the same Gaussian window, $\exp(-Ak^2)$ with $A = 0.05$, centred at the mid-point of the data

range, was used in all cases. Note that the phase correction was not included in the FT, therefore the peak positions are shifted from their true crystallographic values.

3. Calculation of the cluster potential and T-matrix

The reason for the local sensitivity of x-ray absorption spectroscopy is its origin as the result of the photoelectron scattering processes in the potential of atoms surrounding the absorber and the finite lifetime of the photoabsorption process due to the presence of the core-hole and photoelectron lifetime effects [20]. In addition, the thermal vibrations, which exist even in the zero-temperature limit, lead to a significant reduction in the XAFS amplitude for outer coordination shells and also restrict the size of the observed region. The usual range of the x-ray absorption spectroscopy technique is about 5–6 Å.

Thus, the first step in the *ab initio* XAFS calculation is the construction of the total potential for the cluster of some dimension with the centre at the absorbing atom. Then, the local potential around each atom of the cluster can be calculated, and the Schrödinger-like equation can be solved locally by a numerical method. The normalized radial solutions $\mathcal{R}_l$ thus obtained are basic components for the calculation of the scattering T-matrix elements t_l, which define the scattering properties of all the atoms in the cluster.

In this work the MSCALC program, written by Natoli *et al* [7], was used for T-matrix calculations. The single-electron relativistic Dirac equation with two types of local exchange and correlation potentials (ECP), (i) the energy dependent Dirac–Hara (DH) potential and (ii) the complex Hedin–Lundqvist (HL) potential based on the density functional formalism within the single-plasmon pole approximation [21, 22], was solved in a self-consistent way to compute atomic charge densities for each atom in the cluster. Use of the relativistic Dirac–Slater atom code [23] was necessitated by the importance of relativistic corrections for heavy elements like tungsten and rhenium [24]. For the absorbing atom its final state was taken to be fully relaxed with a hole localized in the appropriate core site (in the $2p_{3/2}$ level for the W and Re L_3 edges and in the 1s level for the Mo K edge).

The correction of the XAFS amplitude for the inelastic losses, associated with the lifetime of the photoelectron and the core-hole-level width, has been automatically included in the complex HL ECP to take into account the effect of inelastic losses of the photoelectron in extrinsic channels on plasmon excitations, and it has been approximated by the damping term $\exp(-2R\Gamma/k)$ added to the XAFS formula in the case of the real DH ECP. The core-level widths were taken equal to 3.4 eV for the Re and W L_3 edges and 4.4 eV for the Mo K edge [25].

Three different clusters with parameters shown in table 1 were chosen to describe the crystalline systems studied (ReO_3, $NaWO_3$ and MoO_3). The cluster potential was approximated by a set of spherically averaged muffin-tin (MT) potentials, which were built by following the standard Mattheis prescription [29]: the atomic charge densities obtained from self-consistent solutions of the Dirac equations were placed on each atomic site in the cluster, and the superposed charge density was spherically averaged about the atom whose potential was required, then the Poisson equation for the Coulomb part of the potential was solved, and an appropriate ECP was added. After construction of the scattering MT potentials, the Schrödinger radial equation was solved locally for each atom of the cluster, and the normalized radial solutions

Table 1. Structural data for the cluster potential construction

	ReO_3	$NaWO_3$	MoO_3
Unit cell dimensions			
a (Å)	3.750 [26]	3.860 [27]	13.855 [28]
b (Å)			3.6964
c (Å)			3.9628
Cluster dimensions			
radius (Å)	8.5	8.5	7.2
number of atoms	189	221	77
Muffin-tin radii			
R_{MT}(Me) (Å)	1.0647	1.0959 for W 1.0300 for Na	1.1059
R_{MT}(O) (Å)	0.9978	1.0271	0.9613
Edge	L_3 Re	L_3 W	K Mo

$\mathcal{R}_l$ were obtained. Then, the T-matrix elements t_l were calculated in the usual way by matching the $\mathcal{R}_l$ functions with the solution for free space at the MT radius R_{MT} [30]

$$t_l = \mathrm{i}\frac{\left[kj_l'(kr)\mathcal{R}_l(kr) - j_l(kr)\mathcal{R}_l'(kr)\right]}{\left[kh_l^{+\prime}(kr)\mathcal{R}_l(kr) - h_l^{+}(kr)\mathcal{R}_l'(kr)\right]}\Bigg|_{r=R_{MT}} \tag{1}$$

where j_l and h_l^+ are the spherical Bessel and Hankel functions.

The crystallographic positions of the atoms for the construction of clusters were calculated from data published in [25–27]. We found that in the case of our systems the increase in cluster dimensions around some atom of more than two shells leads to negligible changes in T-matrix elements. Therefore, the radii of clusters were chosen in such way that they included two coordination shells more than is necessary for the interpretation of the easily visible peaks in the FT of the experimental spectrum. In the case of our compounds it corresponded to clusters with radii of ~7–8.5 Å. The values of the MT radii (table 1) were chosen from the Norman criterion [31] and were reduced by a factor ~0.8. The partial covalency of the bond was taken into account by means of the ~10% overlap of the MT spheres.

4. The fast spherical approximation

In the MS theory the oscillatory structure χ^l of the x-ray absorption spectrum can be expanded into the scattering series [2]

$$\chi^l = \sum_{n=2}^{\infty} \chi_n^l \tag{2}$$

where χ_n^l represents the partial contribution from all processes, where the photoelectron, excited on the absorbing atom, experiences $(n-1)$ scatterings by the cluster atoms. It is well known that in many practical cases this series converges

very fast, and thanks to that only the first few parts of it need to be taken into account [8]. The quantities χ_n^l can be expressed in the general functional form [32]

$$\chi_n^l = \sum_i A_i^l(k, R_i) \sin(2kR_i + \Phi_i^l(k, R_i) + 2\delta_c^l) \tag{3}$$

where $\sum_i$ means the sum over all paths of order n starting from and ending at the absorber; R_i indicates the path length; $A_i^l(k, R_i)$ and $\Phi_i^l(k, R_i)$ are the effective amplitude and phase functions, which depend on the wave vector k and the angular momentum l of the photoelectron, the length and geometry of the path and the nature of the scattering centres; δ_c^l is the phase shift due to the absorbing (central) atom.

The first three terms of the series (2) correspond to processes of single (χ_2^l), double (χ_3^l) and triple (χ_4^l) scatterings (SS, DS, TS), and the exact analytical expressions were derived for them earlier in the curved-wave formalism [2, 8]. The formula for the single-scattering case, which was used in our calculations, has the form

$$\chi_2^l = (-1)^l \operatorname{Im}\left[S_0^2 e^{2i\delta_c^l} \sum_j N_j e^{-2\sigma_j^2 k^2} \sum_{\tilde{l}} (-1)^{\tilde{l}}(2\tilde{l}+1) t_{\tilde{l}}^j H(l, \tilde{l}, R_j)\right] \tag{4}$$

with

$$H(l, \tilde{l}, R_j) = \sum_{\tilde{l}} (2\tilde{l}+1) \left\{ \begin{pmatrix} l & \tilde{l} & \tilde{l} \\ 0 & 0 & 0 \end{pmatrix} h_{\tilde{l}}^+(kR_j) \right\}^2$$

where $\begin{pmatrix} l & \tilde{l} & \tilde{l} \\ 0 & 0 & 0 \end{pmatrix}$ is the Wigner $3j$-symbol. The S_0^2 is the amplitude reduction factor owing to multiple-electron excitations. It is less than one and slowly energy-dependent in general case. In this work it was constant at 0.9–1.0. R_j is an average distance from the absorbing atom to the N_j neighbouring atoms in the jth shell, and σ_j is the mean-square radial displacement (the Debye–Waller factor) of the atoms about R_j. t_l is the T-matrix element defined in section 3. The h_l^+ is an outgoing spherical Hankel function. According to Rehr *et al* [33], it can be written in the form of the dimensionless polynomial factor $C_l(\rho)$ that multiplies the asymptotic form of the spherical Hankel function

$$h_l^+(\rho) = i^{-l}(e^{i\rho}/\rho) C_l(\rho) \qquad (\rho = kR). \tag{5}$$

The quantities $C_l(\rho)$ can be found by a recursion method [33] due to that the equation 4 can be calculated fast enough.

In this work we have undertaken the attempt to find a *fast approximation* to the $A_i^l(k, R_i)$ and $\Phi_i^l(k, R_i)$ functions for the double- and triple-scattering terms.

In the plane-wave and short-wavelength limit ($\rho \to \infty$) h_l^+ approaches its asymptotic form, and the exact equations for χ_3^l and χ_4^l can be simplified, so that for one scattering path they take the following forms [8]

$$\begin{aligned}
\chi_3^l &= (-1)^l \left(N S_0^2 e^{-2\sigma_{eff}^2 k^2}/kR_1R_{12}R_2\right) P_l(\cos\theta_c) \\
&\quad \times \operatorname{Im}\left[e^{2i\delta_c^l} e^{2i(R_1+R_{12}+R_2)k} f_1(\alpha, k) f_2(\beta, k)\right] \\
\chi_4^l &= (-1)^l \left(N S_0^2 e^{-2\sigma_{eff}^2 k^2}/kR_1R_{12}R_{23}R_3\right) P_l(\cos\theta_c) \\
&\quad \times \operatorname{Im}\left[e^{2i\delta_c^l} e^{2i(R_1+R_{12}+R_{23}+R_3)k} f_1(\alpha, k) f_2(\beta, k) f_3(\gamma, k)\right]
\end{aligned} \tag{6}$$

where N is the degeneracy of the path, σ_{eff} is the effective Debye–Waller factor, $P_l(\cos\theta_c)$ is the Legendre polynomial, α, β, γ and θ are the angles between bonds, and $f_j(\omega, k)$ is the complex scattering angular-dependent amplitude of jth atom in the cluster. In the PWA the expression for $f(\omega, k)$ has the following form [30]

$$f(\omega, k) = \frac{1}{k}\sum_l (-1)^l (2l+1) t_l P_l(\cos\omega) \tag{7}$$

and the formulae (6) and (7) allow us to compute the MS signal in the plane-wave limit [34].

In the FSA the atoms taking part in the scattering process are considered as *independent weak* modifiers of the spherical photoelectron wave. In this case we can utilize the same formulae as equation (6), but with another form of the scattering amplitudes f_i. Taking into account the curvature of the photoelectron wave, we propose to calculate the scattering amplitude, which will be distance-dependent, according to the expression

$$f(\omega, k, R) = \frac{1}{k}\sum_{\bar{l}} (2\bar{l}+1) t_{\bar{l}} P_{\bar{l}}(\cos\omega) \sum_{\bar{l}} (2\bar{l}+1) \left\{ \begin{pmatrix} l & \bar{l} & \bar{l} \\ 0 & 0 & 0 \end{pmatrix} C_{\bar{l}}(kR) \right\}^2 \tag{8}$$

where R is *the total length of the path from the absorbing (central) atom to the scattering atom*. The main difference of the FSA from previous approaches [8–11,13] arises from the R-dependence of the scattering amplitude function. Usually, R means the distance between two atoms, so that the incoming and outgoing photoelectron waves have radii equal to the distances to the nearest atoms along the scattering path. Thus, each atom in the scattering chain is considered as the final point for the incoming wave and the source of the outgoing wave. In the FSA the influence of atoms on the photoelectron wave is assumed weak, so that they only perturb it. Because of this the quantity R means the wave radius counted out from the absorber atom, which is the wave source, and it is equal to the path length.

The presence of the second sum in equation (8) does not have a very strong effect on the computing time, and formulae (6) and (8) work practically as fast as the PWA, but the agreement with the exact approach [35] is much better. Note that unlike the FCW and the PWA cases, in the FSA, when the photoelectron goes along the chain of atoms the quantities χ_n^l will, in general, be different according to the direction taken. This is due to the form of the R-dependence in equation 8. Thus, if we want to calculate the contribution, for instance, from the double-scattering path $A \to B \to C \to A$, the total χ_n^l signal can be expressed in the FSA as

$$\chi^l_{n\,\text{TOTAL}} = \chi_n^l(A \to B \to C \to A) + \chi_n^l(A \to C \to B \to A). \tag{9}$$

In the case of the FCW or the PWA both directions of the photoelectron wave propagation are equivalent and

$$\chi^l_{n\,\text{TOTAL}} = 2\chi_n^l(A \to B \to C \to A) = 2\chi_n^l(A \to C \to B \to A). \tag{10}$$

This, at first glance unusual fact is only the result of the R-dependence of the scattering amplitude function. It can be interpreted as a mathematical trick of the decomposition of the total $\chi^l_{n\,\text{TOTAL}}(A \to B \to C \to A)$ signal over the set of two

functions $\chi^l_n(A \rightarrow B \rightarrow C \rightarrow A)$ and $\chi^l_n(A \rightarrow C \rightarrow B \rightarrow A)$. In reality, when the scattering process in a chain such as A-B-C-A is considered, only the total signal $\chi^l_{n\text{TOTAL}}$ has physical meaning.

The computer program, called FSA, for the MS calculations both in the FSA and PWA approaches was written by us in FORTRAN-77 and tested on IBM AT-386/387 and VAX computers. The comparative time for the MS term (DS and TS) calculation by the FSA is about 10^3 times shorter than in the case of the FCW method. That is due to more complex form of equations utilized in the FCW approach [7, 8].

5. Examples of the FSA applications

In this section we consider the application of the FSA for the XAFS calculation of three crystalline compounds (ReO_3, $NaWO_3$ and MoO_3). Since their crystallographic structures are well known [26–28], only the Debye–Waller factors are undefined *ab initio* quantities in equations (4) and (6), which were taken as fitting parameters in this work. The precise analysis of the DW factors and their temperature dependence will be published in future.

The choice of these systems was made according to the following criteria:

(i) in all three systems the MS contribution is high due to the presence of the linear and/or close to linear atomic chains;

(ii) the symmetry of the photoelectron is different for the Re and W L_3 edges ($l = 0, 2$) and the Mo K edge ($l = 1$);

(iii) the first two compounds (ReO_3 and $NaWO_3$) have very close cubic structures built from the MeO_6 (Me = Re, W) perfect octahedra joined by corners. They have only a small difference in lattice constants (table 1) and the presence of the Na atoms in the empty spaces between WO_6 octahedra is what principally distinguishes them. The MoO_3 crystal has a layered-type structure built from highly distorted octahedra joined not only by corners but also through ribs. The wide range of Mo–O distances in the first coordination shell makes this structure very asymmetrical from the standpoint of the XAFS calculations. This means that, in contrast to ReO_3 and $NaWO_3$, in the case of MoO_3 there are many non-equivalent scattering paths, which contribute to the total signal and make it more complicated.

5.1. ReO_3

Because of its crystalline structure rhenium oxide is a very convenient compound for testing the MS theory. At atmospheric pressure it has a non-distorted perovskite lattice, which consists of the perfect ReO_6 octahedra joined at the corners with rhenium atoms at the centre and with bonding angle of 180° [26]. Thus, two facts are very interesting from the standpoint of the MS theory. First, the large division of the first (Re–O, R = 1.875 Å) and the second coordination shells (Re–Re, R = 3.75 Å) allows one (under a good signal/noise ratio) to observe between them, in the FT of XAFS, a well isolated peak from the MS processes in the first and the second coordination shells. Secondly, the linear chains (Re–O–Re) lead to a strong focusing effect, which results in a considerable increase of the FT amplitude of the second coordination shell.

The last effect was observed experimentally for the first time by Alberding *et al* [36], but the attempt to explain it in terms of the PWA gave poor agreement

with experiment. More successful results were obtained in later theoretical works based on the SWA formalism. Vedrinskii *et al* [37] have calculated the XAFS for the Re–O–Re chains (with different Re–O–Re angles) with some discrepancies between the experimental [36] and theoretical spectra, which were explained as differences in the FT ranges and inaccuracies in the crystalline potential construction. They have found that the main contributions to the near-edge oscillatory structure are due to the photoelectron scattering in the nearly linear atomic chains originating and terminating at the absorbing centre, but the detailed interpretation of the origin of the peaks in the FT was not given. Note, that besides six rhenium atoms, twenty four oxygen atoms at ~4.19 Å also must contribute to the intense peak of the second coordination shell. In the work of Fritzsche [15], the ratio of amplitudes and the phase differences for the experimental [36] and theoretical spectra are compared. The theoretical amplitude and phase correction factors introduced by Teo [34] were calculated in the RAME and have not reproduced the experimental curves sufficiently well. Thus, a further, more precise interpretation of XAFS in ReO_3 is necessary.

Table 2. Positions of atoms used in the calculation of the main scattering paths in ReO_3. (a is the lattice parameter).

Atom	X (Å)	Y (Å)	Z (Å)
Re_0	0	0	0
O_1	$-\frac{1}{2}a$	0	0
O_2	0	$\frac{1}{2}a$	0
O_3	$\frac{1}{2}a$	0	0
Re_4	a	0	0
O_5	a	$\frac{1}{2}a$	0
Re_6	a	a	0
O_7	$\frac{3}{2}a$	0	0
O_8	a	a	$\frac{1}{2}a$

The atomic positions in the structural model of the ReO_3 crystal, which were employed in the calculation of the XAFS spectrum, are shown in table 2. Due to the high symmetry of the cluster, it is necessary to take only nine atoms into account. They represent the first five coordination shells around the absorbing Re_0 atom.

All possible double- and triple-scattering paths in the first two coordination shells and single-scattering paths up to the fifth shell were calculated. The main paths with a contribution to the total signal of more than 1% and their degeneracies are included in table 3. Comparison of the calculated spectra with experimental data for the HL ECP is shown in figure 1. The agreement is good enough over the whole energy range. Note that the use of the HL ECP leads to an accurate value of the amplitude at low energies.

To understand how different paths contribute to the total spectrum, let us look at figures 2 and 3, where the separate signals from the SS, DS and TS paths and their FT are shown.

One can see that the single-scatterings from the rhenium and oxygen atoms give contributions in different parts of the energy range: the oxygens at low energies and the rheniums at high energies. This is due to the peculiarities of their backscattering amplitudes which is a well known fact for any light and heavy atoms [24]. Note that the oxygen atoms located as far as in the third and fifth coordination shells also give

Table 3. The main scattering paths used in the calculation of the rhenium L_3 edge XAFS in ReO_3. The numbers used in the paths correspond to the atoms in table 2

Type	Name	Path	Degeneracy
Single	XSS1	0–1–0	6
scattering	XSS2	0–4–0	6
χ_2	XSS3	0–5–0	24
	XSS4	0–6–0	12
	XSS5	0–7(8)–0	30
Double	XDS1	0–1–2–0	24
scattering	XDS2	0–1–3–0	6
χ_3	XDS3	0–3–4–0	12
	XDS4	0–3–5–0	48
Triple	XTS1	0–1–0–1–0	6
scattering	XTS2	0–1–0–2–0	24
χ_4	XTS3	0–1–0–3–0	6
	XTS4	0–3–4–3–0	6
	XTS5	0–3–4–7–0	12

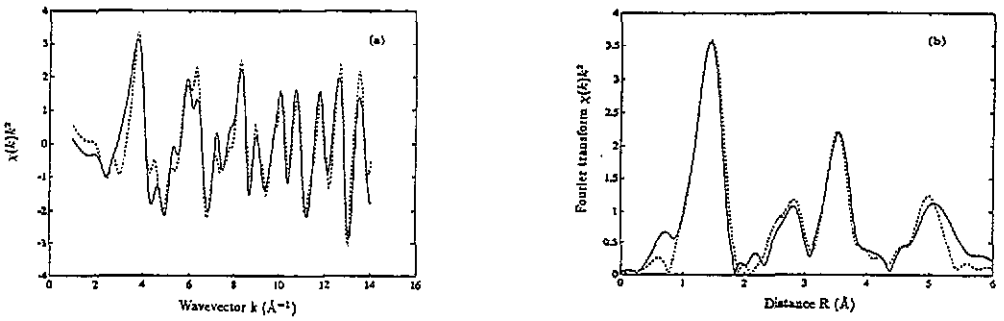

Figure 1. Experimental (dashed line) and calculated with HL ECP (solid line) curves for the rhenium L_3 edge in ReO_3: (*a*) the XAFS $\chi(k)k^2$; (*b*) Fourier transforms with the Gaussian window.

a sufficiently large contribution to the total signal, compared with the rhenium atoms, due to their large number.

Among MS contributions the linear paths both in the first (O_1–Re_0–O_3) and in the second (Re_0–O_3–Re_4) coordination shells are the most important. This is due to the focusing role of the atom (Re_0 or O_3) in the middle of the chain, whose sufficiently high forward-scattering amplitude leads to a considerable increase in the final signal. It should also be noted that in the case of the L_3 edge such paths as $Re_0 \rightarrow O_1 \rightarrow O_2 \rightarrow Re_0$ and $Re_0 \rightarrow O_1 \rightarrow Re_0 \rightarrow O_2 \rightarrow Re_0$ (see table 3) also contribute in the low-energy region in contrast to L_1 or K-edges when they vanish because of the $P_l(\cos\theta)$ term in equations (6), which is equal zero for $l=1$ and angle $\theta=90°$.

Now an interpretation of the main peaks in the FT (see, figure 3) can be made. The first peak at 1.4 Å corresponds to the six nearest oxygen atoms in the first coordination shell and can be calculated in the single-scattering approximation. The next peaks located in the range from 2.2 to 4.2 Å cannot be decomposed into separate contributions due to their overlap. It can only be mentioned that the left-hand side of the peak at 2.2–3.1 Å is due to the DS $Re_0 \rightarrow O_1 \rightarrow O_2 \rightarrow Re_0$ path in the first shell. Its

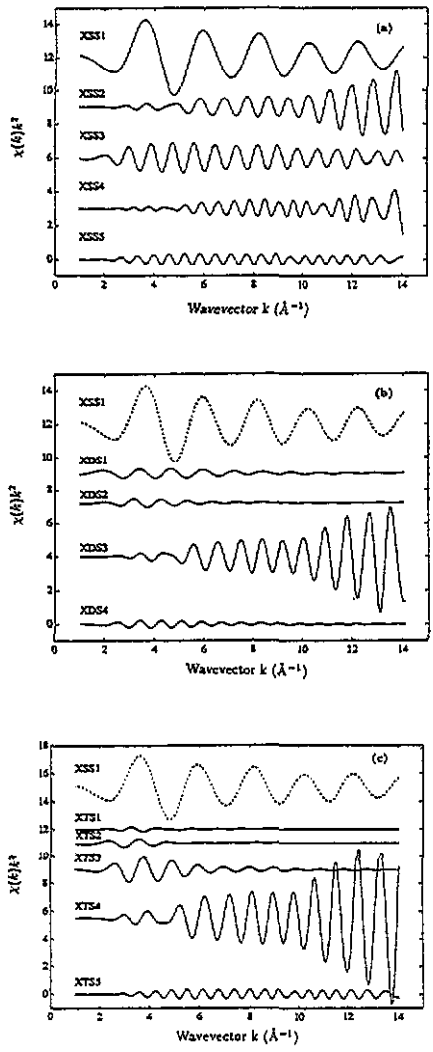

Figure 2. Single- (*a*), double- (*b*) and triple- (*c*) scattering contributions (see table 3) to the total XAFS signal, calculated with HL ECP and zero values of the Debye–Waller factors. In figures (*b*) and (*c*) the SS signal (dashed line) of the first coordination shell is shown for comparison.

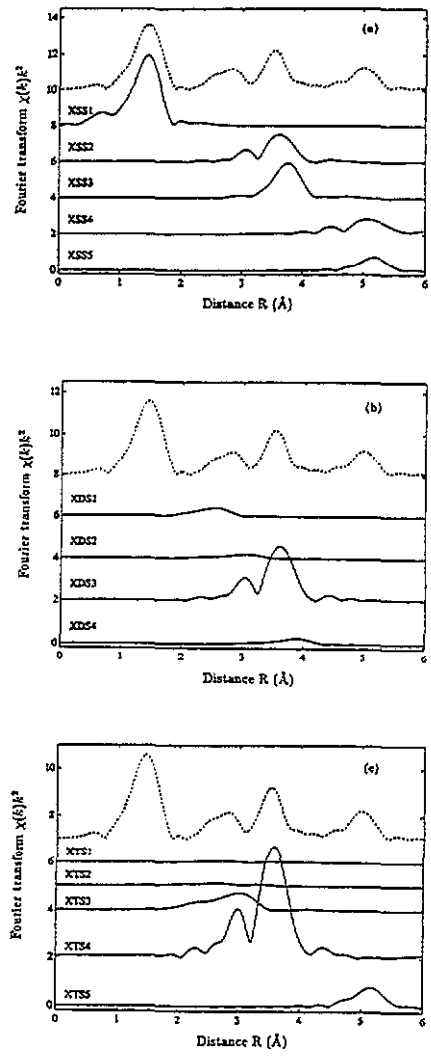

Figure 3. Fourier transforms with the Gaussian window of the curves shown in figure 2. The dashed line is experiment.

right-hand side is due to other MS processes in the first coordination shell, especially in the linear chain O_1–Re_0–O_3, but in the main due to the contribution of the DS and TS processes in the Re_0–O_3–Re_4 chain. The last ones are also the main reason for the large amplitude of the peak at 3.5 Å . In addition, the single scatterings from the rhenium and oxygen atoms in the second and third shells make a contribution to the peak at 3.5 Å too. The last sufficiently wide peak at 5 Å is due to the single scatterings from the rhenium and oxygen atoms in the fourth and fifth coordination shells and the TS process in the Re_0–O_3–Re_4–O_7 chain with the double focusing effect first on the oxygen (O_3) and then on the rhenium (Re_4) atoms.

5.2. $NaWO_3$

$NaWO_3$ tungsten bronze has a structure that is very close to ReO_3 [27]. It is built from the WO_6 perfect octahedra joined at the corners with sodium atoms in the empty spaces between them. Around the tungsten atom there are six oxygen atoms with the W–O distance equal to 1.930 Å in the first coordination shell and eight sodium atoms with the W–Na distance equal to 2.236 Å.

In the work of Studer *et al* [38], only the first two coordination shells around the tungsten were analysed in the single-scattering approximation. The structural parameters for the first shell are in a good agreement with x-ray diffraction data, but the data for the second shell differ quite strongly. The reason for this is the strong influence of multiple-scattering effects in the W–O–W chains on the amplitude and phase of the XAFS spectrum. Thus, the present work is the first study of $NaWO_3$ by the multiple-scattering approach.

Table 4. Positions of atoms used in the calculation of the main scattering paths in $NaWO_3$. (a is the lattice parameter)

Atom	X (Å)	Y (Å)	Z (Å)
W_0	0	0	0
O_1	$-\frac{1}{2}a$	0	0
O_2	0	$\frac{1}{2}a$	0
O_3	$\frac{1}{2}a$	0	0
W_4	a	0	0
O_5	a	$\frac{1}{2}a$	0
W_6	a	a	0
O_7	$\frac{3}{2}a$	0	0
O_8	a	a	$\frac{1}{2}a$
Na_9	$\frac{1}{2}a$	$\frac{1}{2}a$	$\frac{1}{2}a$
Na_{10}	$\frac{3}{2}a$	$\frac{1}{2}a$	$\frac{1}{2}a$
W_{11}	a	a	a

The atomic positions in the structural model of the $NaWO_3$ crystal, which were used in the calculation of the XAFS spectrum, are shown in table 4. Due to the high symmetry of the cluster, it is necessary to take only eleven atoms into account. They represent the first seven coordination shells around the absorbing W_0 atom.

All possible double- and triple-scattering paths in the first three coordination shells and single-scattering paths up to the seventh shell were calculated. Comparison of the calculated spectra with experimental data for the HL ECP is shown in figure 4. The agreement is good enough in all energy ranges. The main paths with a contribution to the total signal of more than 1% and their degeneracies are included in table 5.

On the whole the origin of all the peaks in the FT of the W L_3 edge XAFS in $NaWO_3$ is similar to the ReO_3 case. There are, however, several distinctions. The main difference between these two structures, the presence of sodium atoms in $NaWO_3$, does not affect very strongly the shape of the total signal. The reason for this is the greater value of the thermal damping factor (or the Debye–Waller factor) for $NaWO_3$, which one can see from the comparison of the experimental XAFS spectra and their FT for $NaWO_3$ and ReO_3. It could seem that sodium atoms placed in the second coordination shell can be the cause of the strong MS effects in such chains as

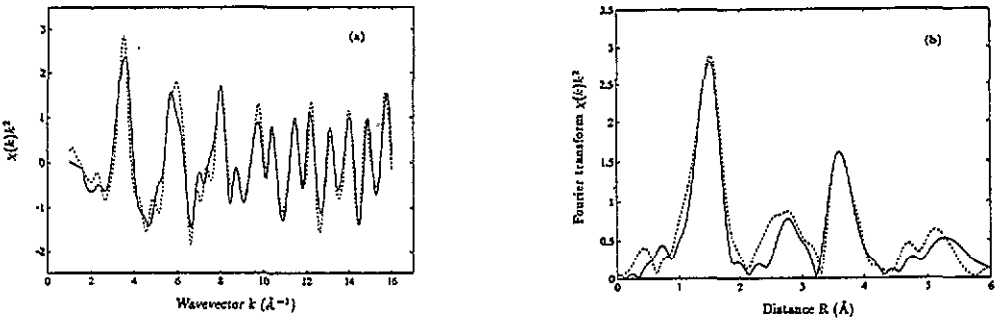

Figure 4. Experimental (dashed line) and calculated with HL ECP (solid line) curves for the tungsten L_3 edge in $NaWO_3$: (*a*) the XAFS $\chi(k)k^2$; (*b*) Fourier transforms with the Gaussian window.

Table 5. The main scattering paths used in the calculation of the tungsten L_3 edge XAFS in $NaWO_3$. The numbers, used in paths, correspond to atoms in table 4

Type	Name	Path	Degeneracy
Single-scattering χ_2	XSS1	0–1–0	6
	XSS2	0–9–0	8
	XSS3	0–4–0	6
	XSS4	0–5–0	24
	XSS5	0–6–0	12
	XSS6	0–7(8)–0	30
	XSS7	0–10–0	24
Double-scattering χ_3	XDS1	0–1–2–0	24
	XDS2	0–1–3–0	6
	XDS3	0–3–4–0	12
	XDS4	0–3–5–0	48
	XDS5	0–9–11–0	8
Triple scattering χ_4	XTS1	0–1–0–1–0	6
	XTS2	0–1–0–2–0	24
	XTS3	0–1–0–3–0	6
	XTS4	0–3–4–3–0	6
	XTS5	0–3–4–7–0	12
	XTS6	0–9–11–9–0	8

Na–W_0–Na and W_0–Na–W, in analogy to oxygens. Their calculated signals are greatly broadened and do not practically contribute to the total spectrum. Thus, only the SS signal from sodium atoms in the second shell is significant. It contributes to the FT at 3 Å and leads to further complication of the structure in that region.

5.3. MoO_3

The study of multiple-scattering effects in XAFS of MoO_3 is presented for the first time. In previous works [17,39], only the first coordination shell has been studied in the single-scattering approximation, and the obtained set of distances is in a good agreement with x-ray diffraction data [28].

The MoO_3 crystal has a layered-type structure built from highly distorted octahedra joined by corners as well as through ribs [28]. The wide set of Mo–O distances in the first coordination shell, which is well observed as the splitting of the

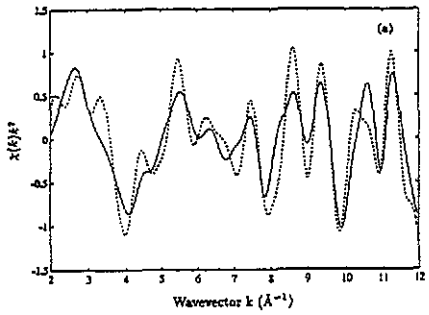

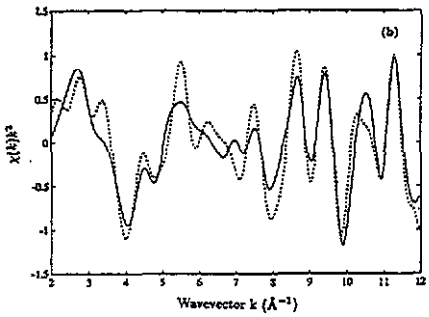

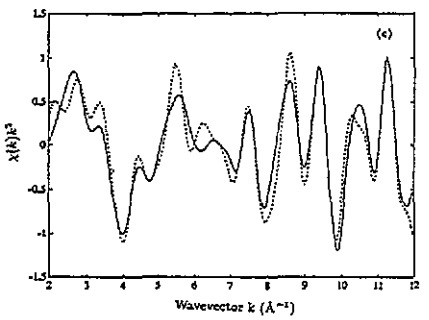

Figure 5. Experimental (dashed line) and calculated with HL ECP (solid line) curves for the molybdenum K edge in MoO_3: (*a*) only SS contribution; (*b*) SS + DS contributions; (*c*) SS + DS + TS contributions.

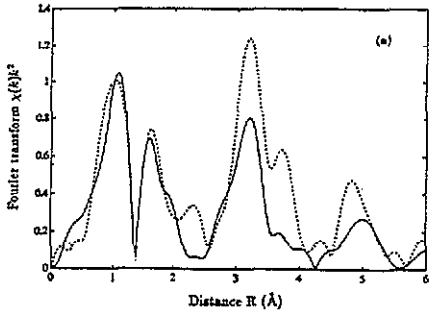

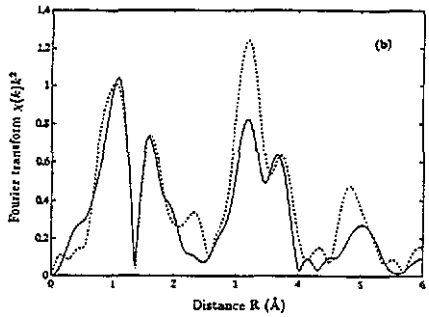

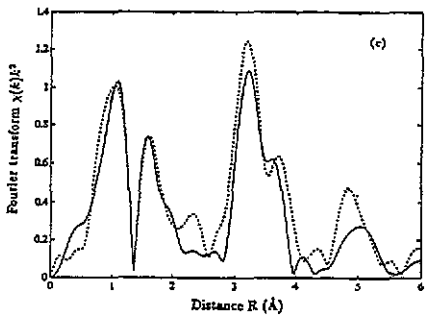

Figure 6. Fourier transforms with the Gaussian window of the curves shown in figure 5.

first peak in the FT (figure 5), makes this structure very asymmetrical and leads to an availability of many non-equivalent scattering paths, which contribute to the total spectrum and make it more complicated.

The large separation between two layers defined by the lattice parameter a = 13.855 Å leads to that the XAFS in MoO_3 is formed only by atoms lying in one layer. The bonding angles between neighbouring molybdenum atoms have the following values: ~110° and ~143° in the plane formed by octahedra joined through ribs and ~163° in the perpendicular direction, in which octahedra are joined by corners. Although there are no exactly linear chains as in both previous compounds, the MS contribution is very important in this case too. To show this, the XAFS calculations

with both the HL and DH ECP were done by first taking into account only the SS paths (figures 5(*a*) and 7(*a*)). After that, the DS paths (figures 5(*b*) and 7(*b*)) and the TS paths (figures 5(*c*) and 7(*c*)) within the first two coordination shells were added successively. It is clear that the addition of the DS and TS contributions improves the agreement between experimental and calculated curves. This fact is easily seen in figures 6 and 8, where the FT are displayed. Note that the change of the HL ECP by the DH ECP leads to the slight modification of the amplitude and phase of signal. In the first two cases of the ReO_3 and $NaWO_3$ crystals the effect was smaller and appeared only at small energies.

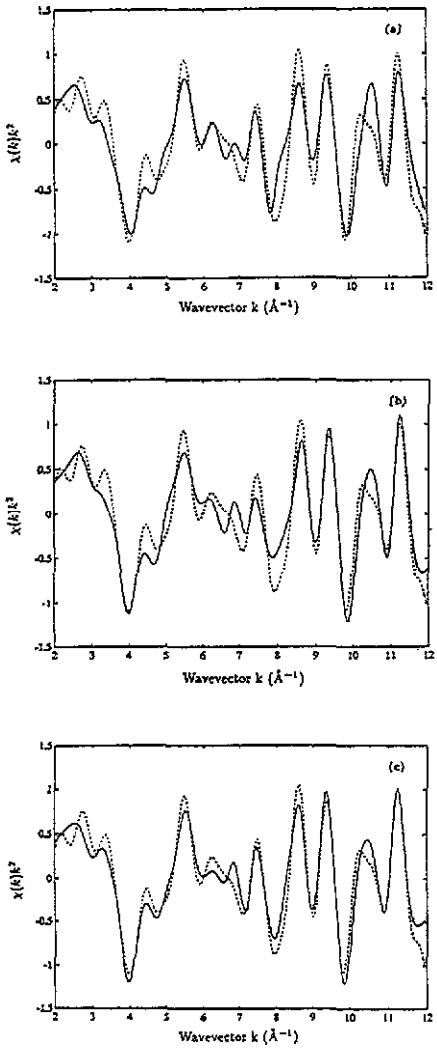

Figure 7. Experimental (dashed line) and calculated with DH ECP (solid line) curves for the molybdenum K edge in MoO_3: (*a*) only SS contribution; (*b*) SS + DS contributions; (*c*) SS + DS + TS contributions.

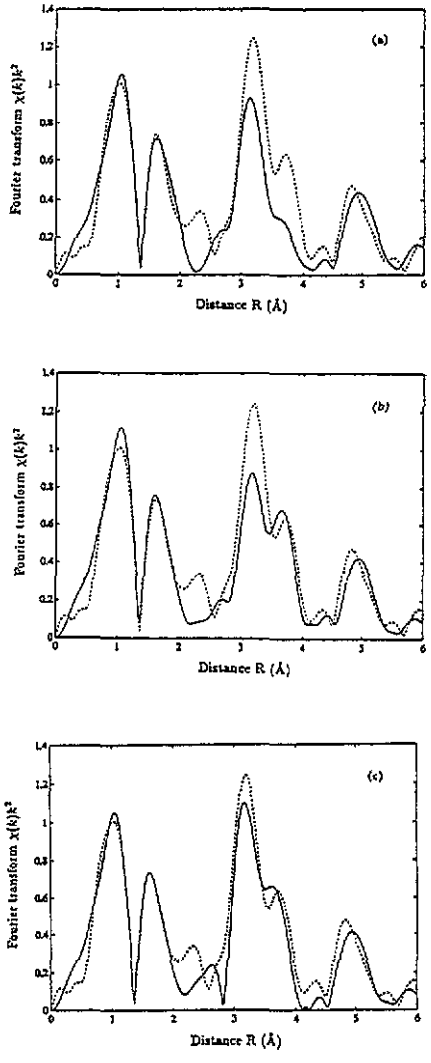

Figure 8. Fourier transforms with the Gaussian window of the curves shown in figure 7.

The first two peaks located in the range from 0.5 to 2.2 Å correspond to a very

distorted first coordination shell, where two groups of distances can be distinguished [17, 28]: the short bonds (1.67 and 1.73 Å) correspond to the peak at 1.0 Å and the long bonds (1.95×2, 2.25 and 2.33 Å) correspond to the peak at 1.8 Å. The intensive double peak located in the range from 2.5 to 4.0 Å corresponds to the molybdenum atoms in the second coordination shell, joined with the central molybdenum atom by corners as well as through ribs, and the oxygen atoms in the third coordination shell. Its amplitude depends from the MS contributions in the Mo–O–Mo chains. The last peak at 5 Å is due to the SS processes in the outer (molybdenum and oxygen) shells.

6. Summary

We have presented the new fast spherical approximation for the calculation of multiple-scattering contributions in the x-ray absorption fine structure. The detailed interpretation of the Re L_3 edge XAFS in ReO_3, the W L_3 edge XAFS in $NaWO_3$ and the Mo K edge XAFS in MoO_3 has been performed in the framework of the FSA approach. The analysis of the MS effects in XAFS of $NaWO_3$ and MoO_3 has been done for the first time. The agreement obtained with experiment is good in all energy ranges. Note that the FSA is a very fast computational method, so we conclude that it can be used in routine experimental analysis.

Acknowledgments

We wish to thank the Italian National Synchrotron Centre at Frascati for hospitality and support during our stay there. We are also thankful to Professors C R Natoli and M Benfatto and Dr T A Tyson for the opportunity to use the MSCALC program in our calculations and fruitful discussions. We would like to show our gratitude to Professor E Burattini and his collaborators for the opportunity to carry out experiments on the PWA EXAFS station. We also thank the group of Professor G Dalba (University of Trento) for stimulating discussions.

References

[1] Lee P A, Citrin P H, Eisenberger P and Kincaid B M 1981 *Rev. Mod. Phys.* **53** 769
[2] Natoli C R and Benfatto M 1986 *J. Physique* **47** 11
[3] Filipponi A, Di Cicco A, Benfatto M and Natoli C R 1990 *Europhys. Lett.* **13** 319
[4] Motta N, De Crescenzi M and Balzarotti A 1983 *EXAFS and Near Edge Structure* ed A Bianconi *et al* (Berlin: Springer) p 103
[5] Lee P A and Pendry J B 1975 *Phys. Rev.* B **11** 2795
[6] Ashley C A and Doniach S 1975 *Phys. Rev.* B **11** 1279
[7] Ruiz-Lopez M F, Loops M, Goulon J, Benfatto M and Natoli C R 1988 *Chem. Phys.* **121** 419
[8] Gurman S J, Binsted N and Ross I 1986 *J. Phys. C: Solid State Phys.* **19** 1845
[9] Fritzsche V and Rennert P 1986 *Phys. Status Solidi* b **135** 49
[10] Fritzsche V 1990 *J. Phys.: Condens. Matter* **2** 1413
[11] Gurman S J 1988 *J. Phys. C: Solid State Phys.* **21** 3699
[12] Boland J J, Crane S E and Baldeschwieler J D 1982 *J. Chem. Phys.* **77** 142
[13] Rehr J J and Albers R C 1990 *Phys. Rev.* B **41** 8139
Mustre J, Yacoby Y, Stern E A and Rehr J J 1990 *Phys. Rev.* B **42** 10 843
[14] Hung N V 1989 *Exp. Tech. Phys.* **37** 203
[15] Frizsche V 1989 *J. Phys.: Condens. Matter* **1** 7715

[16] McKale A G, Veal B W, Paulikas A P, Chan S K and Knapp G S 1988 *J. Am. Chem. Soc.* **110** 3763
[17] Balerna A, Bernieri E, Burattini E, Kuzmin A, Lusis A, Purans J and Cikmach P 1991 *Nucl. Instrum. Methods* **A308** 234
[18] Teo B K 1986 *EXAFS: Basic Principles and Data Analysis* (Berlin: Springer)
[19] Victoreen J A 1948 *J. Appl. Phys.* **19** 855
[20] Stern E A 1974 *Phys. Rev.* B **10** 3027
[21] Chou S H, Rehr J J, Stern E A and Davidson E R 1984 *Phys. Rev.* B **35** 2604
[22] Hedin L and Lundqvist B I 1971 *J. Phys. C: Solid State Phys.* **4** 2064
[23] Desclaux J P 1975 *Comput. Phys. Commun.* **9** 31
[24] Teo B K and Lee P A 1979 *J. Am. Chem. Soc.* **101** 2815
[25] Keski-Rahkonen O and Krause M O 1974 *At. Data Nucl. Data Tables* **14** 140
[26] Jørgensen J E, Jørgensen J D, Batlogg B, Remeika J P and Axe J D 1986 *Phys. Rev.* B **33** 4793
[27] Wyckoff R W G 1963 *Crystal Structures* vol 1 2nd edn (New York: Wiley)
[28] Kihlborg L 1963 *Ark. Kemi* **21** 357
[29] Mattheiss L 1964 *Phys. Rev.* A **134** 970
[30] Schiff L I 1955 *Quantum Mechanics* 2nd edn (New York: McGraw–Hill)
[31] Norman J G 1974 *Mol. Phys.* **81** 1191
[32] Benfatto M and Natoli C R 1987 *J. Non-Cryst. Sol.* **95 & 96** 319
[33] Rehr J J, Albers R C, Natoli C R and Stern E A 1986 *Phys. Rev.* B **34** 4350
[34] Teo B K 1981 *J. Am. Chem. Soc.* **103** 3990
[35] Kuzmin A, Purans J, Benfatto M and Natoli C R 1992 *Phys. Rev.* B **47**
[36] Alberding N, Crozier E D, Ingals R and Houser B 1986 *J. Physique* **47** 681
[37] Vedrinskii R V, Bugaev L A and Levin I G 1988 *Phys. Status Solidi* b **150** 307
[38] Studer F, Lebail A and Raveau B 1986 *J. Solid State Chem.* **63** 414
[39] Mensch C T J, van Veen J A R, van Wingerden B and van Dijk M P 1988 *J. Phys. Chem.* **92** 4961